ESCUELA DE CIENCIAS
DEPARTAMENTO DE GEOLOGÍA

TRABAJO DIRIGIDO DE GRADO

MAGNETIC FABRIC OF THE COMBIA FORMATION

ALEJANDRA TABARES GRAJALES

Trabajo dirigido de Grado presentado como requisito parcial para optar al Tıtulo de Geóloga

Asesorado por

MARIA ISABEL MARÍN-CERÓN, PhD
VICTOR ANDRÉS PIEDRAHITA VÉLEZ

MEDELLIN
2018

MAGNETIC FABRIC OF THE COMBIA FORMATION

Tabares, A.[a], Marín-Cerón, M.I.[a], Piedrahita, V. A. [a]

[a] Departamento de Ciencias de la Tierra, Universidad Eafit, Medellín, Colombia.

ABSTRACT

The Mio-Pliocene Combia Formation consists of pyroclastic deposits and lava flows which were formed and emplaced under the active Late-Cenozoic geological context of the northern Andes. Here, we present new magnetic fabric of two stratigraphical sequences of pyroclastic rocks, the Anzá-Bolombolo (AB) section and the Metida Creek (MC) section, and another section of lava flows, the Cerro Amarillo (CA) section. Anisotropy of magnetic susceptibility (AMS) data of the AB section characterize flow directions from the SE, whilst the MC succession is identified by flow directions towards the SE-ESE. These flow patterns suggest volcanic plugs in the central Amagá Basin. These old volcanoes would have been located in the areas of Titiribí and/or Venecia. However, according to previous geomorphological characterizations and paleo-current studies, intrusive rocks of the Venecia town are more likely to be the main volcanic necks in the central Area of the Amagá Basin. The CA section has flow directions towards the SW, characterizing proximal volcanic vents to the section. Despite the fact that the Combia Formation may have been affected by Late-Cenozoic deformational events recorded in the Amagá Basin, our AMS data only reflect flow directions. Therefore, further studies are necessary to characterize deformations on the volcanic and volcano-clastic rocks of the Combia Formation.

1. Introduction

Rock magnetic studies of volcanic and volcano-clastic rocks provide useful information for paleogeographic reconstructions, basin analyses and stratigraphical correlations (Tarling and Hrouda, 1993; Borradaile and Henry, 1997). Furthermore, mechanisms of transport-deposition, deformational features, and location of volcanic vents of volcanic and volcano-clastic rocks have been studied through paleomagnetic and magnetic fabric data (e.g Elwood et al., 1982; Incoronato et al., 1983; MacDonald and Palmer, 1990; Palmer et al., 1991; Le Pennec et al., 1998; Ort et al., 2003; Pioli et al., 2008).

The inter-Andean valley between the Western and Central Cordilleras of Colombia so called the Cauca Depression (Fig. 1) is an area occupied by a series of Cenozoic sedimentary basins, which were formed in an active geological context in the northern Andes of South America (Barrero et al, 2007; Sierra and Marín-Cerón, 2011). Tectonic processes as plate subduction and terrane accretion are involved in the geological evolution of the sedimentary basins located in the Cauca Depression (Acosta, 1978; Alfonso et al., 1994; Cediel et al., 2003; Sierra and Marín-Cerón, 2011).

The northern area of the Cauca Depression is occupied by the Amagá Basin (Fig. 1), which is a sedimentary basin structurally controlled by the Cauca-Romeral Fault System and closely located to the western boundary of the South American Plate (Sierra and Marín-Cerón, 2011). Important geological events in the northern Andes of South America, as the Andean Orogeny and the Panama-Choco Block (PCB) collisional stages, are partially recorded by deformational features of Cenozoic rocks of the Amagá Basin (Piedrahita et al., 2017a; Piedrahita et al., 2017b). The Cenozoic rocks of the Amagá Basin include the sedimentary infill of the basin, which consist of the Oligocene-Miocene Amagá Formation and the Mio-Pliocene Combia Formation, and a series of Mio-Pliocene hypabyssal intrusives which are associated with a volcanic event named Combia Event (Fig. 2) (Grosse, 1926; Van der Hammen, 1958; Leal-Mejía et al., 2011; Montes et al., 2015; Mesa-García, 2015; Piedrahita et al., 2017a).

The deformational history of the Amagá Formation has been mainly described through rock magnetic data. Magnetic fabric studies in the fluvial Amagá Formation characterized a structural regime with NW-SE compression and NE-SW simple shear, which caused syn- and post- depositional deformation in the Oligocene-Miocene Amagá Formation (Piedrahita et al., 2017a). Additionally, paleomagnetism records from the Mio-Pliocene Combia hypabyssal intrusives show that those rocks suffered counterclockwise rotations about a vertical axis of 20.2°±10.7° and local tilting (Piedrahita et al., 2017b). These rock magnetic data characterized reactivations of the Cauca-Romeral Fault System which have been triggered by the Late-Cenozoic interaction between the PCB and the Northern Andean Block (NAB). Other geochronological, thermochronological and stratigraphical works (e.g. Van der Hammen, 1958; Cediel et al., 2003; Silva et al., 2008; Restrepo-Moreno et al., 2009; Lara et al., 2015; Montes et al., 2015) have supported those conclusions reached by paleomagnetism and magnetic fabric data. Furthermore, those geological studies have also identified the influence of other tectonic events, as the Andean Orogeny, over the geological evolution of the Amagá Basin.

Despite the fact that the Cenozoic rocks of the Amagá Basin functions as an archive of important tectonic events occurred in the northern Andes, the Mio-Pliocene Combia Formation, which consist of a series of volcanic and volcano-clastic rocks (Grosse, 1926; Calle and González, 1980), have remained as a unit whose emplacement and deformational features have not been studied. Therefore, the locations of the volcanic vents which generated the Combia Formation are unknown. Furthermore, the possible Mio-Pliocene deformations of this unit, and their associations with the Late-Cenozoic geological events which have affected the northern Andes of South America have not been analyzed.

The study of the Combia Formation can allow gaining new information related to the geological evolution of the Amagá Basin and the Mio-Pliocene tectonic context which affected the northern Andes of South America. Therefore, this work seeks to identify deformational features and/or volcanic vents of the Combia Formation through a new dataset of magnetic fabric and magnetic mineralogy data. Our new data describes the

emplacement and flow mechanisms of the Combia Formation. Furthermore, the timing of intracontinental deformation in the Amagá Basin can be tentatively constrained.

2. Geological framework

The Mio-Pliocene geological framework of the northern Andes of South America was related to major Cenozoic tectonic events as the subduction of the Caribbean and Nazca Plates beneath the South American Plate, and the collisional stages of the allochthonous Panama-Choco Block (PCB) against the northwestern margin of the Northern Andean Block (NAB) (Case et al., 1971; Pennington, 1981; Taboada et al., 2000; Cediel et al., 2003; Farris et al., 2011; Villagómez and Spikings, 2013; Farris et al., 2017).

The NAB, which is located within the South American Plate, is a geologically-differentiated segment of the Andean Chain. This tectonic block can be divided into two contrasted fringes with continental affinity rocks to the east and oceanic affinity rocks to the west. The western area of the NAB includes several NNE-SSW trending terranes as the Romeral Terrane. The basement of this terrane mainly consists of oceanic affinity rocks, however, some areas have been described as mélange zones (Gansser, 1973; Cediel et al., 2003). The Romeral Terrane is limited by strike-slip faults which have had several Meso-Cenozoic reactivation periods (Ego and Sébrier, 1995; Chicangana, 2005; Vinasco and Cordani, 2012). The eastern limit of the Romeral Terrane is the Romeral Fault, which is characterized by separating the continental basement of the northern Andes from a series of oceanic affinity rocks (Case et al., 1971; Chicangana, 2005). On the other hand, the western area of the Romeral Terrane is bounded by the Cauca Fault, which is a suture zone between Mesozoic terranes of oceanic affinity (Cediel et al., 2003). These faults are extended between central Colombia and Ecuador and form the Cauca-Romeral Fault System (Fig. 2) (Kammer, 1993; Cediel et al., 2003; Chicangana, 2005).

The Cauca-Romeral Fault System have had several strike-slip reactivations, with alternating left-lateral and right-lateral motion, during the early Miocene, late Miocene, Pleistocene and Holocene (Ego and Sébrier, 1995; Chicangana, 2005; Vinasco and Cordani,

2012). These deformational events have been related to the collisional stages of the PCB against the northwestern corner of the South American Plate (Restrepo-Moreno et al., 2009; Vinasco and Cordani, 2012; Piedrahita et al., 2017a; Piedrahita et al., 2017b). The PCB consists of Meso-Cenozoic subduction-related and oceanic plateau igneous rocks (de Boer et al., 1991; Buchs et al., 2011; Wegner et al., 2011). These rocks are separated from the NAB through the Uramita Fault Zone, which is characterized by its transpressional behavior and left-lateral component (Duque-Caro, 1990; Mann and Corrigan, 1990; Mann and Kolarsky, 1995). The PCB collided with the NAB in E-SE direction during several stages between the Paleogene and Neogene (Farris et al., 2011; Piedrahita et al., 2017a; Farris et al., 2017). These collisional stages are associated with the closure of the Central America seaway which connected the Atlantic and Pacific Oceans. Therefore, this tectonic event had important oceanographic, climatic and biotic implications (Jaramillo, 2016; O'Dea et al., 2016).

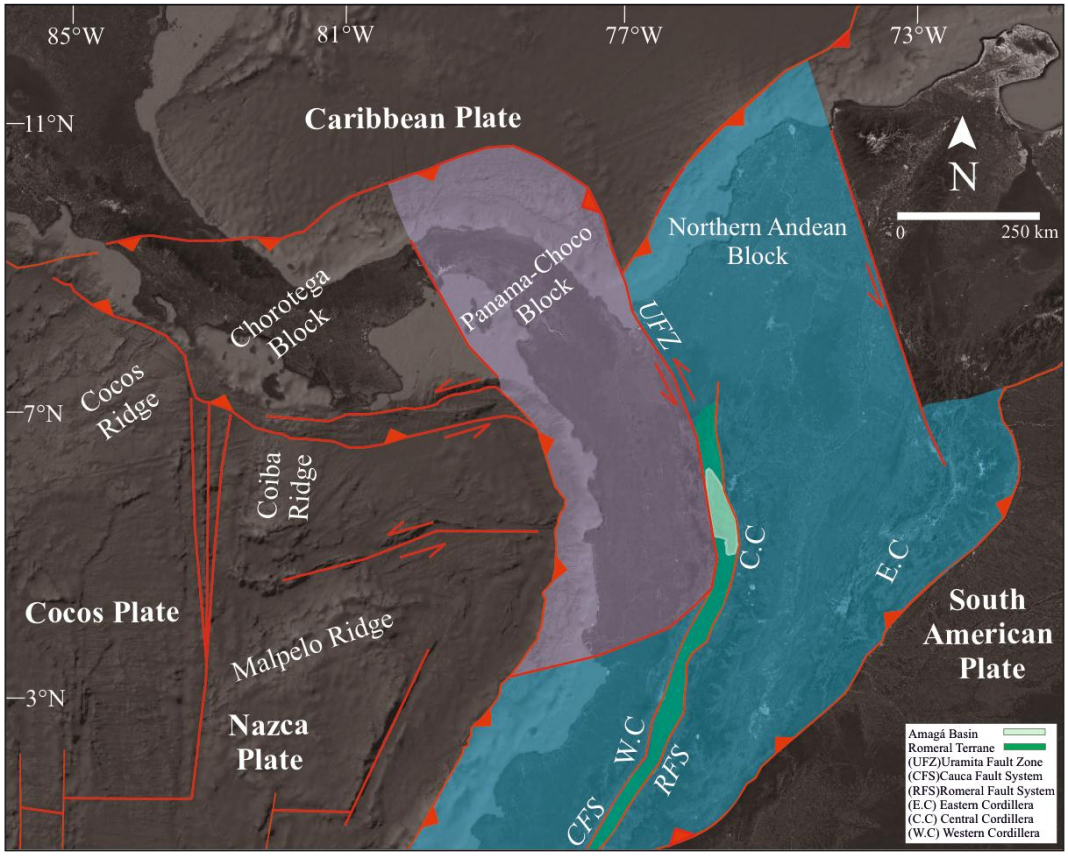

Fig.1. Tectonic framework of the northern Andes of South America including principal tectonic blocks, faults and the Amagá Basin.

Despite its geological repercussions, the timing of the collision of the PCB against northwestern Colombia is still discussed. Montes et al. (2015) suggest a ~15 Ma final collisional stage of the PCB to the northwestern area of the NAB. This hypothesis is based on the presence of Eocene zircon crystals with "Panamanian signature" in Middle-Miocene sedimentary rocks located within the northern Andes. On the other hand, O'Dea et al. (2016), through a detailed review of the available oceanographic, molecular and geochronological data, showed that a Middle-Miocene total closure of the Central America seaway was not possible, characterizing a Pliocene-Pleistocene age for the final collisional event of the PCB and identifying a current strain of this block over the northwestern South American Plate (Cortés and Angelier, 2005; O'Dea et al., 2016).

The PCB collisional stages against the northwestern corner of the NAB, in addition to the Cenozoic subduction of the Nazca Plate beneath the South American Plate, caused mountain-building, volcanism, and reactivation periods of fault systems in the northern Andes. A significant consequence of these major tectonic events was a series of Middle-Late Cenozoic magmatic and volcanic episodes which include the Combia magmatism (Duque-Caro, 1990; Cediel et al., 2003; Mesa-García, 2015; Marín-Cerón et al., 2018). This magmatic/volcanic event, characterized by subduction-related products with tholeiitic and calc-alkaline geochemical signatures in volcanic, volcano-clastic and hypabyssal rocks (Mesa-García, 2015; Borrero and Toro-Toro, 2016; Marín-Cerón et al., 2018), is preceded by ~24-20 Ma igneous intrusions whose records are located to the west of the Cauca Fault. The Mio-Pliocene interaction between the PCB and the western sector of the NAB led to an eastward migration of that Early-Miocene (~24-20 Ma) magmatic belt to the Cauca Depression. Thereby, the ~12-6 Ma Combia Event was generated (Duque-Caro, 1990; Cediel et al., 2003; Marín-Cerón et al., 2018).

The Combia event, and other consequences of the PCB accretionary stages as intracontinental deformation and rock exhumation are partially recorded in the Amagá Basin (Sierra and Marín-Cerón, 2011; Piedrahita et al., 2017a). The Amagá Basin is located in the mélange zone of the Romeral Terrane between the Central and Western Cordilleras of Colombia (Cediel et al., 2003; Sierra and Marín-Cerón, 2011). The basement of this

basin consists of low-grade metamorphic rocks as schists and phyllites whose ages have not been clearly assigned, therefore, they have been mapped as low-grade metamorphic rocks with pre-Cenozoic ages. In fault contact with those metamorphic rocks, there are several Triassic intrusives with gabbroic, dioritic and granitic compositions. Furthermore, a series of volcanic and sedimentary Cretaceous oceanic affinity rocks as basalts, diabases and pyroclastic rocks interlayered with cherts and siltstones are also in fault contact with the other rocks which constitute the basement of the Amagá Basin. Several Cretaceous intrusives also appear in this area, however, these rocks are mainly located in the adjacent cordilleras which enclose the Amagá Basin (Fig. 2) (Grosse, 1926; Calle and González, 1980; Calle et al., 1980; Sierra and Marín-Cerón, 2011).

The crystalline rocks of the basement of the Amagá Basin are covered by sedimentary units, as the Amagá and Combia Formations, and intruded by the Combia hypabyssal rocks (Fig. 2). The Amagá Formation is divided into two members, the Oligocene-Early Miocene Lower Member and the middle to late Miocene Upper Member (Van der Hammen, 1957; Montes et al., 2015; Piedrahita et al., 2017). Both members are constituted by sedimentary rocks formed in fluvial environments (Silva et al., 2008). On the other hand, the Combia Formation consists of volcanic and volcano-clastic rocks, which are split between a volcanic member and a sedimentary member. The volcanic member of the Combia Formation is characterized by lava flows with basaltic and andesitic compositions, and a series of pyroclastic flows with ashes, tuffs and volcanic breccias. The sedimentary member of the Combia Formation consists of conglomerates, sandstones and siltstones whose source areas are the volcanic and volcano-clastic rocks of the volcanic member of this unit (Grosse, 1926; Calle and González, 1980). The thickness of both members of the Combia Formation has not been clearly identified, nevertheless, Calle and González (1980) have described sequences of ~600m for the volcanic member and ~270m for the sedimentary member.

The Combia event also generated a series of hypabyssal rocks whose record is in the central and southern area of the Amagá Basin (Ramírez et al., 2006; Calle and González, 1980; Borrero and Toro-Toro, 2016). These rocks intrude the Amagá Formation, however, their

field relationship with the Combia Formation are not clear. Based on paleo-current analyses and geomorphological observations, it has been thought that the Combia hypabyssal rocks correspond to remnants of volcanic plugs in the Amagá Basin (Álvarez, 1973; Ramírez et al., 2006).

The age of the Combia Event has been assigned through U-Pb ages and zircon and apatite fission track ages. U-Pb ages of 7.6 ± 0.2 Ma and 7.6 ± 0.3 Ma for hypabyssal rocks (Leal-Mejía, 2011) and 8.58 ± 0.22 Ma, 8.55 ± 0.18 Ma and 8.44 ± 0.17 Ma for volcano-clastic rocks have been found in the Combia Formation (Díaz and Cuellar, 2017).

This work study three sequences of the Combia Formation, the Anzá-Bolombolo (AB) section, the Cerro-Amarillo (CA) section and the Metida Creek (MC) section. Mesa-Garcia (2015) provides stratigraphical, ZFT, AFT and geochemical data for these stratigraphical successions (see below) (Fig. 4).

The MC section (~45m thick) is located in the western area of the Amagá Basin and consists of well-dated layers of pyroclastic rocks with SW strikes and intermediate inclinations towards the NW. Several strata have sedimentary structures as bioturbation, ripple lamination and cross-bedding. The bottom of the MC succession is occupied by lapilli-tuff breccias, tuffs and a subordinated layer of pyroclastic flows. The AFT ages of these rocks range from 19.7 ± 9.5 Ma to 5.1±2.5 Ma, whilst the ZFT are between 12.1±2.0 Ma and 6.1±1.1 Ma. At the middle of the sequence, tuffs with AFT ages of 15.9±11.1 Ma and ZFT ages between 10.1±2.1 Ma and 6.2±2.6 Ma, appear juxtaposed by a lapilli tuff breccia with a ZFT age of 6.7±1.5 Ma, and a lapilli tuff with an AFT age of 8.3±3.1 Ma. The top of the MC sequence has not been dated and is constituted by lapilli tuffs, tuffs, tuff breccias and tuffaceous sandstones (Fig. 4a).

The CA sequence (~170m thick) is closely located to the eastern margin of the Amagá Basin. This folded succession consists of tilted tabular layers (NS/50W) of ignimbrites at the bottom, basalts at the middle and pyroclastic breccias at the top (Fig. 4b). The CA succession has not been dated, in spite of this fact, a Mio-Pliocene age for the rocks of this

section has been assigned due to their tholeiitic geochemical signature and compositional similitudes with other rocks of the Combia event (Mesa-Garcia; 2015). According to Mesa-García (2015), the CA deposits correspond to a stratovolcano which characterized an effusive phase of the Combia Event. Therefore, volcanic products of the CA section would have remained near the volcanic vent. Some layers of the CA section present oriented vesicles which could be used to infer flow directions.

The AB section is the shortest sequence studied in this work and is located in the western area of the Amagá Basin. It corresponds to a sequence of ~11m of thickness with horizontal layers oriented towards the SW. The bottom of the AB succession is constituted by interlayered tuffs and lapilli tuffs with AFT ages of 12.1 ± 6.9. Those rocks are juxtaposed by pyroclastic deposits which are separated between them by erosional contacts. At the top of the AB section, there are volcanic agglomerates and breccias with AFT ages of 7.9 ± 2.1, and undifferentiated lava flows (Fig. 4c) (Mesa-Garcia; 2015).

The Amagá Basin is affected by the Cauca-Romeral Fault System and their expressions (Fig. 2). The different behavior and structural style of the faults belonged to this system characterize at least two deformational events in the basin (Calle and González, 1980; Piedrahita et al., 2017b). The western Amagá Basin is structurally controlled by the strike-slip Sabanalarga Fault, which is the easternmost fault trace of the Cauca Fault (Calle and González, 1980). The central and eastern areas of the Amagá Basin are characterized by NNW-SSE faults as the Cascajosa Fault, the Amagá Fault and the Piedecuesta Fault. These faults have allegedly had normal and reverse reactivation periods (Grosse, 1926; Calle and González, 1980; Mejía et al., 1988). In the southern sector of the Amagá Basin, it is found the Arma Fault, which is a NW-trending structure with oblique normal left-lateral behavior (Acosta et al., 2007). Outside the Amagá Basin, in the western flank of the Central Cordillera of Colombia, the main trace of the Romeral Fault System and its easternmost expression, the San Jeronimo Fault, are identified (Grosse, 1926). These faults have had several strike-slip and reverse reactivation periods linked to the Meso-Cenozoic tectonic activity of the northern Andes (Chicangana, 2005; Vinasco and Cordani, 2011).

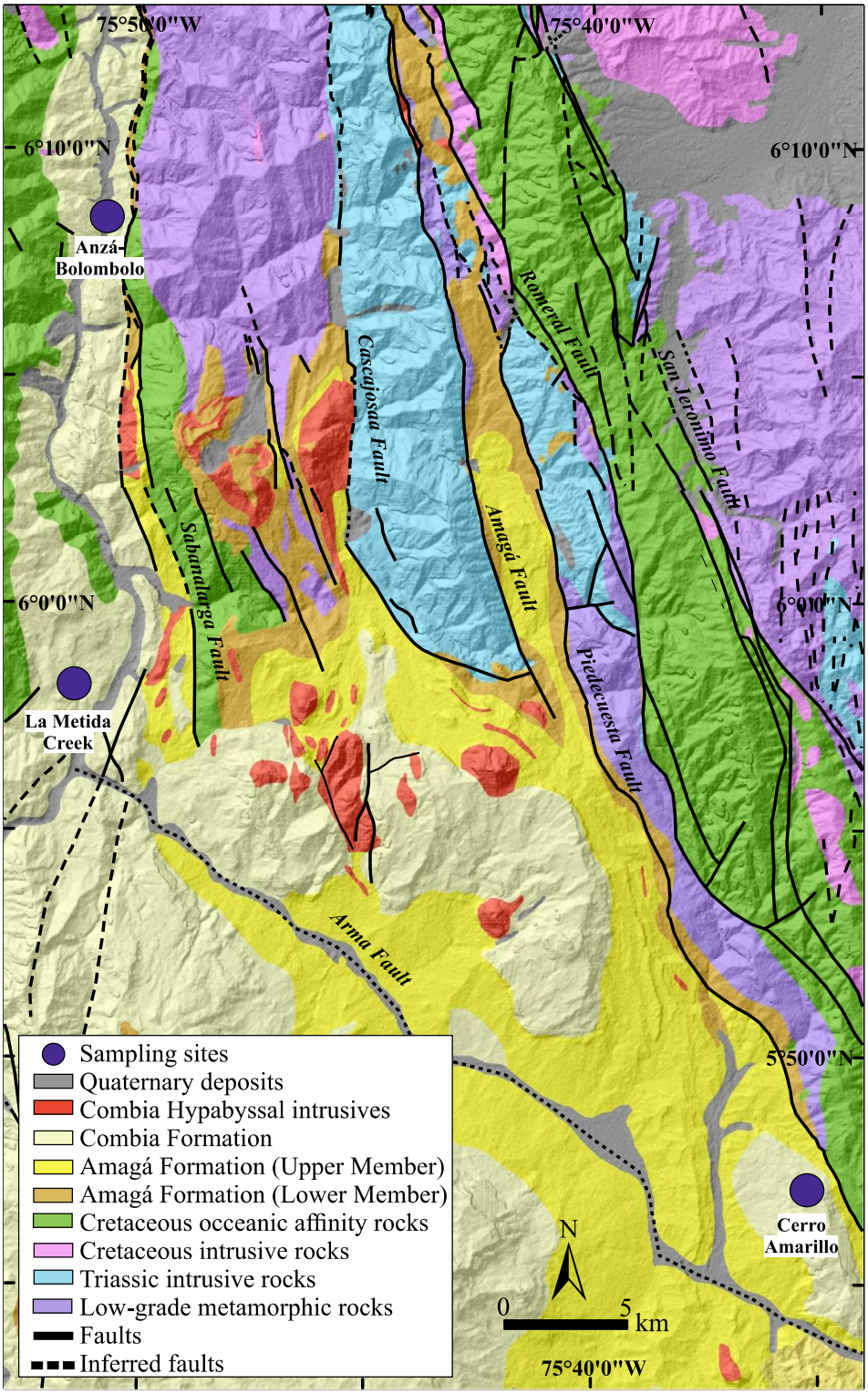

Fig.2. Geological map of the study area (Calle et al., 1980) showing sampling sites used in this study.

3. Methodology

3.1 Magnetic mineralogy

In order to test the presence of minerals whose magnetic susceptibility depends on the field (i.e pyrrhotite) (Worm et al., 1993; Pokorny et al., 2004). We have measured the bulk susceptibility of nine samples in fields of 2 A/m, 12.5 A/m, 25 A/m, 50 A/m, 100 A/m, 200 A/m, 300 A/m, 400 A/m and 600 A/m using a Kappabridge MFK1-FB at the the Laboratorio de paleomagnetismo of the Universidad Eafit (Medellin, Colombia). We have generated bulk magnetic susceptibility (k) vs field (H) curves for six (6) samples of the MC section, two (2) samples of the CA section, and one (1) sample of the AB section.

3.2 Anisotropy of magnetic susceptibility (AMS)

For this magnetic fabric study, oriented cylindrical cores were extracted from three (3) stratigraphical successions of the Combia Formation using a gasoline-powered portable drill. They were obtained between 4 and 10 cores with 2.5 cm in diameter, which were subsequently cut into specimens of 2.2 in height to yield a total of 240 standard cylindrical specimens.

In order to obtain the AMS tensor, a sequence of 15 directional magnetic susceptibility measurements was performed using the rotational design of Jelinek (1977). AMS measurements were performed using a Kappabridge MFK1-FB at the Laboratorio de paleomagnetismo of the Universidad Eafit (Medellin, Colombia). Our data was processed with software Anisoft 4.2 (Chadima and Jelinek, 2009) and presented as mean tensor statistics (Jelinek, 1981).

The orientation and magnitude of the three (3) main axes were determined to define the magnetic fabric. The shape of the AMS ellipsoid was analyzed through the shape parameter (T), which ranges from -1 (linear magnetic fabrics) to 1 (planar magnetic fabrics) (Jelinek, 1981). The intensity of the preferred orientation of the minerals which control the magnetic

fabric is given by the anisotropy degree (P_j) (Jelinek, 1981) and the bulk magnetic susceptibility is expressed using the mean magnetic susceptibility (K_m) (Nagata, 1961).

Equations of the quantitative parameters used to describe AMS ellipsoids are defined as follows:

$T = [2\mathrm{In}(K_1/K_2) / \mathrm{In}(K_1/K_2)] - 1$ (Jelinek, 1981)

$P_j = \exp(2[(\eta_1-\eta_m)^2 + (\eta_2-\eta_m)^2 + (\eta_3-\eta_m)^2])^{1/2}$ (Jelinek, 1981)

Where $\eta_1 = \ln K_1$, $\eta_2 = \ln K_2$, $\eta_3 = \ln K_3$ and $\eta_m = (\eta_1 \cdot \eta_2 \cdot \eta_3)^{1/3}$

$Km = (K_1 + K_2 + K_3)/3$ (Nagata, 1961)

4. Results

4.1 Magnetic mineralogy

Our *k*(H) curves and K_m-P_j plot clearly distinguish two groups of data (Fig. 3a, b). The first group is only constituted by samples from the MC section. This group of samples characterizes *k*(H) curves with field-independent susceptibilities, whose values range from 2.78×10^{-4} in the sample JJ2-14-4-1 to 1.80×10^{-3} in the sample JJ2-6-1-2 (Fig. 3a). The K_m-P_j plot displays that samples from the MC section have relatively low K_m and P_j values. K_m values are mainly between 500×10^{-6} SI and 1000×10^{-6} SI. However, some samples of the MC section have higher K_m values which up to ~2000×10^{-6} SI, and lower values near ~200×10^{-6} SI. The highest K_m values are characterized by pyroclastic flows from the MC section. P_j values are also low, they are ranging between 1.002 and 1.060 and do not present any relationship with K_m (Fig. 3a).

The second group of data, which includes the AB and CA sections, has magnetic susceptibility values considerably higher than the MC section. *k*(H) curves show a really slight positive tendency between H and *k* for samples JJ1-6-1 (CA section), JJ4-2-1 (CA ssection) and JJ2-1-17 (AB section). *k* values range from 2.66×10^{-2} (2 A/m) to 2.94×10^{-2}

(600 A/m) in the sample JJ1-6-1, from 2.09 × 10^{-2} (2 A/m) to 2.09 × 10^{-2} (600 A/m) in the sample JJ4-2-1, and from 2.17 × 10^{-2} (2 A/m) to 2.23 × 10^{-2} (600 A/m) in the sample JJ2-1-17 (Fig. 3a). The K_m-P_j plot displays low P_j values for samples from CA and AB sections. These values are between 1.007 and 1.062 and are similar to the P_j values found in rocks from the MC succession. On the other hand, K_m values from the CA and AB section are between ~15300 × 10^{-6} SI and ~38220 × 10^{-6} SI and are considerably higher than K_m values from the MC sequence (Fig. 3b).

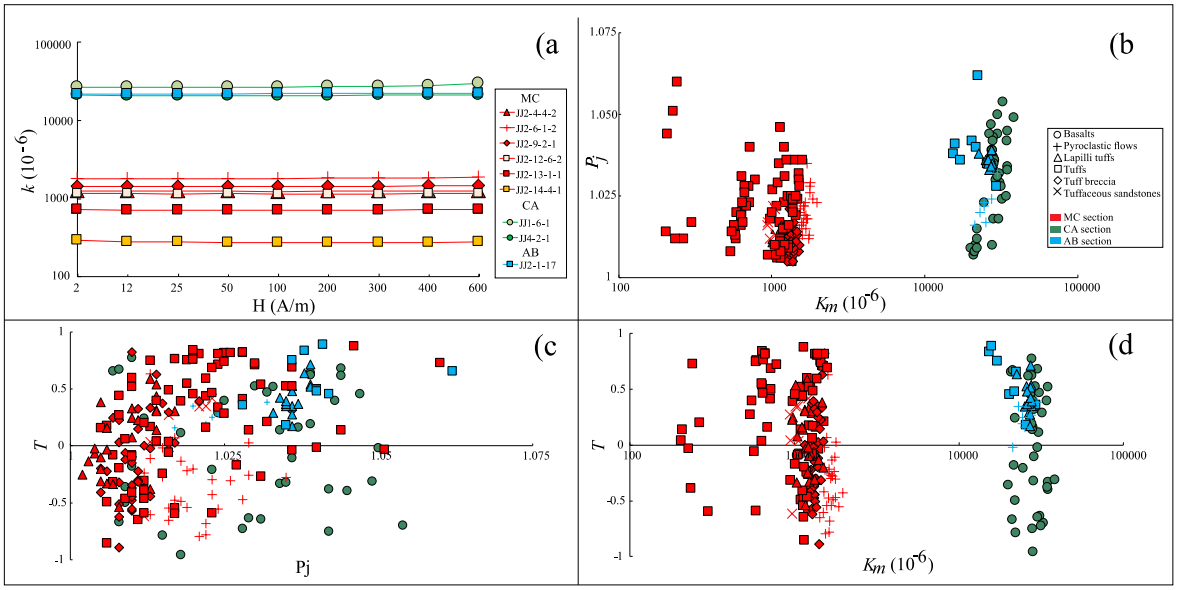

Fig. 3. a). k measured as a function of applied field with the intensity gradually increased. b). K_m - P_j plot. c). P_j – T plot. d). K_m - T plot.

4.2 Magnetic fabric

Magnetic fabric measurements characterize almost isotropic samples. Anisotropy degree ranges from 0.02% (1.002) to 6% (1.062) and does not have any relationship with other AMS parameters as K_m or T (Fig. 3b, c, d). The highest P_j values are identified in tuffs from the MC and AB sections, and basalts from the CA sequence. On the other hand, the lowest P_j values belong to tuff breccias and tuffs from the MC succession and basalts from the CA section (Fig. 3b, c).

The T parameter is widely variable and does not have any relationship with other AMS parameters as P_j or Km. For the successions CA and MC, prolate, neutral and oblate fabrics are observed, whilst for the AB section, only neutral to oblate fabrics have been characterized. In general, a slight predominance of oblate ellipsoids can be identified for the measured specimens (Tab.1; Fig. 3c, d).

The MC section was sampled in 14 layers of pyroclastic flows. At the center of the section, tuffs of the sites QM-JJ2-14, QM-JJ2-13 and have variable magnetic directional data. The prolate fabric of the site QM-JJ2-14 has a sub-horizontal SE-trending magnetic lineation and a sub-vertical magnetic foliation plane with NW-SE strike. The site QM-JJ2-13, which has an oblate fabric, is characterized by an NE-trending K_1 with an intermediate plunge. The magnetic foliation of this site (QM-JJ2-13) has an intermediate inclination which is dipping towards the NW, describing a plane with NE-SW strike. Finally, the site QM-JJ2-12 has an oblate fabric which defines a NW-trending magnetic lineation with intermediate plunges. The magnetic foliation of this site has a NW-SE strike with an intermediate dip towards the SW (Fig. 4a).

The prolate fabrics of the sites QM-JJ2-11 (tuffs) and QM-JJ2-10 (tuff breccia), and the oblate fabric of the site QM-JJ2-09 (tuff breccia) are characterized by WSW to NW-trending magnetic lineation with sub-vertical plunges at site QM-JJ2-11, and intermediate to sub-horizontal inclinations at sites QM-JJ2-10 and QM-JJ2-09. The magnetic foliation plane of these sites is also similar. K_{min} defines planes with NE-SW strikes and NW dips, however, the inclination of these planes is sub-vertical at sites QM-JJ2-11 and QM-JJ2-10, and sub-horizontal at site QM-JJ2-09 (Fig. 4a).

The sites QM-JJ2-08 (tuffaceous sandstone), QM-JJ2-07 (lapilli tuff), QM-JJ2-06 (pyroclastic flow), QM-JJ2-05 (tuff), and QM-JJ2-04 (lapilli tuff) have similar magnetic fabrics in terms of shape and magnetic directional data. Only the site QM-JJ2-08 has a neutral magnetic fabric, the remaining sites have oblate ellipsoids. All of these sites describe WNW to SW trending magnetic lineations.

									Geographic Coordinate System							Paleogeographic Coordinate System					
Site	Rock Type	n	Km	St. Deviation	Pj	St. Deviation	T	St. Deviation	K1	Conf. Angle	K2	Conf. Angle	K3	Conf. Angle	Strike/Dip	K1	Conf. Angle	K2	Conf. Angle	K3	Conf. Angle
AB-JJ2-1	Tuff	7	0.0202	0.00486	1.021	0.01	0.551	0.205	325.7/17.1	50.3/23.9	233.8/6.0	48.7/37.7	125.1/71.8	38.1/30.3	205/3	325.3/14.7	50.3/23.9	234.1/4.6	48.7/37.7	127.0/74.7	38.1/30.3
AB-JJ2-2	Lapilli tuff	16	0.0264	0.0013	1.026	0.002	-0.006	0.151	139.5/20.7	15.6/11.6	230.6/2.9	30.0/14.4	328.1/69.1	30.0/10.7	205/3	140.0/23.4	15.6/11.6	230.7/1.6	30.0/14.4	324.3/66.5	30.0/10.7
AB-JJ2-3	Pyroclastic flow	7	0.0251	0.00281	1.009	0.005	0.089	0.134	121.6/38.9	81.9/27.6	221.5/12.0	81.9/22.3	325.4/48.6	29.3/25.9	205/3	121.9/41.9	81.9/27.6	222.1/11.1	81.9/22.2	323.8/46.0	29.3/25.9
CA-JJ1	Basaltic andesite	14	0.032	0.00355	1.016	0.013	-0.147	0.522	215.8/36.3	37.5/16.1	321.2/19.8	34.6/27.2	73.8/47.0	28.5/24.5	180/50	-	-	-	-	-	-
CA-JJ3	Basaltic andesite	10	0.0283	0.0013	1.035	0.005	0.624	0.164	321.1/0.70	32.6/5.20	230.6/36.0	32.7/14.90	52.0/54.0	15.50/5.60	175/52	-	-	-	-	-	-
CA-JJ4	Basaltic andesite	7	0.0212	0.000707	1.005	0.002	0.455	0.546	211.2/4.6	62.7/11.8	60.2/84.8	62.5/21.1	301.4/2.5	25.2/13.2	175/52	-	-	-	-	-	-
CA-JJ5	Basaltic andesite	7	0.0286	0.000946	1.035	0.006	-0.216	0.371	35.9/49.6	11.1/5.80	243.2/37.1	10.8/7.1	142.6/13.7	8.0/5.3	180/50	-	-	-	-	-	-
MC-JJ2-4	Lapilli tuff	13	0.00125	0.000137	1.003	0.002	-0.268	0.237	282.6/1.4	15.4/6.7	191.7/34.5	39.4/9.2	14.6/55.5	39.2/6.1	200/42	100.3/40.2	15.4/5.4	219.6/30.0	39.9/9.3	333.7/35.2	39.7/6.1
MC-JJ2-5	Tuff	21	0.00121	0.000136	1.01	0.012	-0.299	0.398	272.9/36.3	39.3/18.5	33.9/35.1	62.3/35.2	152.7/34.4	62.3/27.6	200/42	96.3/4.3	39.3/18.5	3.3/34.0	62.3/35.2	192.6/55.6	62.3/27.6
MC-JJ2-6	Lapilli tuff breccia	27	0.00165	0.000122	1.017	0.006	-0.549	0.303	230.1/27.8	13.8/9.2	336.5/28.2	29.6/10.2	103.7/48.5	29.6/12.3	205/50	241.8/0.7	13.8/9.2	151.6/11.7	29.6/10.2	334.8/78.3	29.6/12.3
MC-JJ2-7	Lapilli tuff	13	0.00113	0.000105	1.008	0.002	-0.033	0.251	277.2/63.2	27.7/12.3	47.1/17.9	43.7/18.0	143.6/19.2	41.0/11.2	205/50	286.8/14.2	27.7/12.3	24.6/28.2	43.6/18.1	173.1/57.8	41.0/11.9
MC-JJ2-8	Tuffaceous sandstone	7	0.00103	0.0000948	1.007	0.004	0.028	0.359	217.1/0.90	53.7/27.0	308.6/56.9	56.3/40.2	126.5/33.1	46.5/26.9	210/55	34.8/5.3	53.7/27.0	304.7/2.2	56.3/40.2	192.4/84.3	46.5/27.0
MC-JJ2-9	Lapilli tuff breccia	22	0.00133	0.0000779	1.008	0.004	0.333	0.406	297.5/37.4	40.3/14.1	27.8/0.40	39.8/12.1	118.4/52.6	17.6/10.4	210/55	117.9/17.6	40.3/14.1	208.4/1.6	39.8/12.1	303.2/72.4	17.6/10.5
MC-JJ2-10	Lapilli tuff breccia	15	0.00137	0.0000797	1.006	0.001	-0.405	0.341	257.1/21.5	25.6/20.5	17.2/51.8	38.1/17.5	154.0/29.9	36.9/24.5	210/55	77.5/20.4	25.6/20.5	339.9/19.7	38.1/17.5	209.5/61.0	36.9/24.5
MC-JJ2-11	Tuff	11	0.00144	0.0000763	1.015	0.005	-0.143	0.072	260.9/77.1	9.5/3.8	39.9/9.8	44.6/9.4	131.4/8.3	44.6/3.8	210/55	291.1/24.7	9.5/3.8	27.5/13.7	44.6/9.4	144.1/61.3	44.6/3.8
MC-JJ2-12	Tuff	16	0.00115	0.0000987	1.004	0.004	0.627	0.421	312.5/29.5	73.0/20.4	204.4/28.9	73.2/31.0	79.0/46.4	38.3/20.4	195/63	132.0/27.7	73.0/20.4	224.8/5.3	73.1/31.1	324.7/61.8	38.3/20.4
MC-JJ2-13	Tuff	19	0.000642	0.0000637	1.014	0.008	0.718	0.372	32.9/26.7	57.3/14.7	274.8/43.1	57.6/22.0	143.6/35.1	27.4/11.8	195/63	357.0/26.7	57.3/14.7	97.1/19.3	57.6/22.0	218.5/56.2	27.4/11.8
MC-JJ2-14	Tuff	7	0.00024	0.0000335	1.016	0.021	-0.867	0.428	135.6/12.3	27.7/20.1	265.8/71.4	85.1/19.9	42.5/13.8	85.1/23.4	195/63	173.9/57.8	27.7/20.1	278.9/9.3	85.1/19.9	14.4/30.5	85.1/23.4

Tab. 1. AMS data of the studied sections.

Plunges of K_1 axis are variable and describe sub-vertical inclinations at site QM-JJ2-07, intermediate inclinations at sites QM-JJ2-06 and QM-JJ2-05, and sub-horizontal inclinations at sites QM-JJ2-08 and QM-JJ2-04.

Magnetic foliation planes between these sites are also similar. These planes have NE-SW strikes at sites QM-JJ2-08, QM-JJ2-07, QM-JJ2-06, QM-JJ2-05, with dips towards the NW and intermediate inclinations. Only the site QM-JJ2-07 presents a sub-vertical magnetic foliation plane (Fig. 4a).

The site QM-JJ2-04 is characterized by a magnetic foliation plane with a different attitude regarding the other sites located at the top of the MC section. This site has a NW-SE magnetic foliation plane which is dipping ~45° towards the SW (Fig. 4a).

The AB section was sampled in three layers. The site AB-JJ2-1 consists of a tuff with an oblate fabric characterized by a sub-horizontal magnetic lineation oriented towards the NW and a sub-horizontal magnetic foliation dipping towards the NW. The remaining sites, AB-JJ2-2 (lapilli tuffs) and AB-JJ2-3 (pyroclastic flows), are identified by neutral magnetic fabrics with SE-trending lineations and sub-horizontal to intermediate plunges. The magnetic foliations of these sites have sub-horizontal to intermediate dips which are related to awell-clustered K_3 axis with NW orientations (Fig. 4c).

The CA succession was sampled at 4 layers of basaltic andesites, two of these sampling sites have oriented vesicles towards the SW, indicating flow directions from the NE. The oblate magnetic fabric of the site CM-JJ1 and the prolate magnetic fabric of the site CM-JJ4 are characterized by SW-trending magnetic lineations with sub-horizontal and intermediate plunges. The site CM-JJ1has a magnetic foliation plane which is dipping towards the SW and has a NW-SE strike. On the other hand, the site CM-JJ4 has a sub-horizontal K_{min} which is associated with a sub-vertical magnetic foliation plane with NE-SW strike (Fig. 4b).

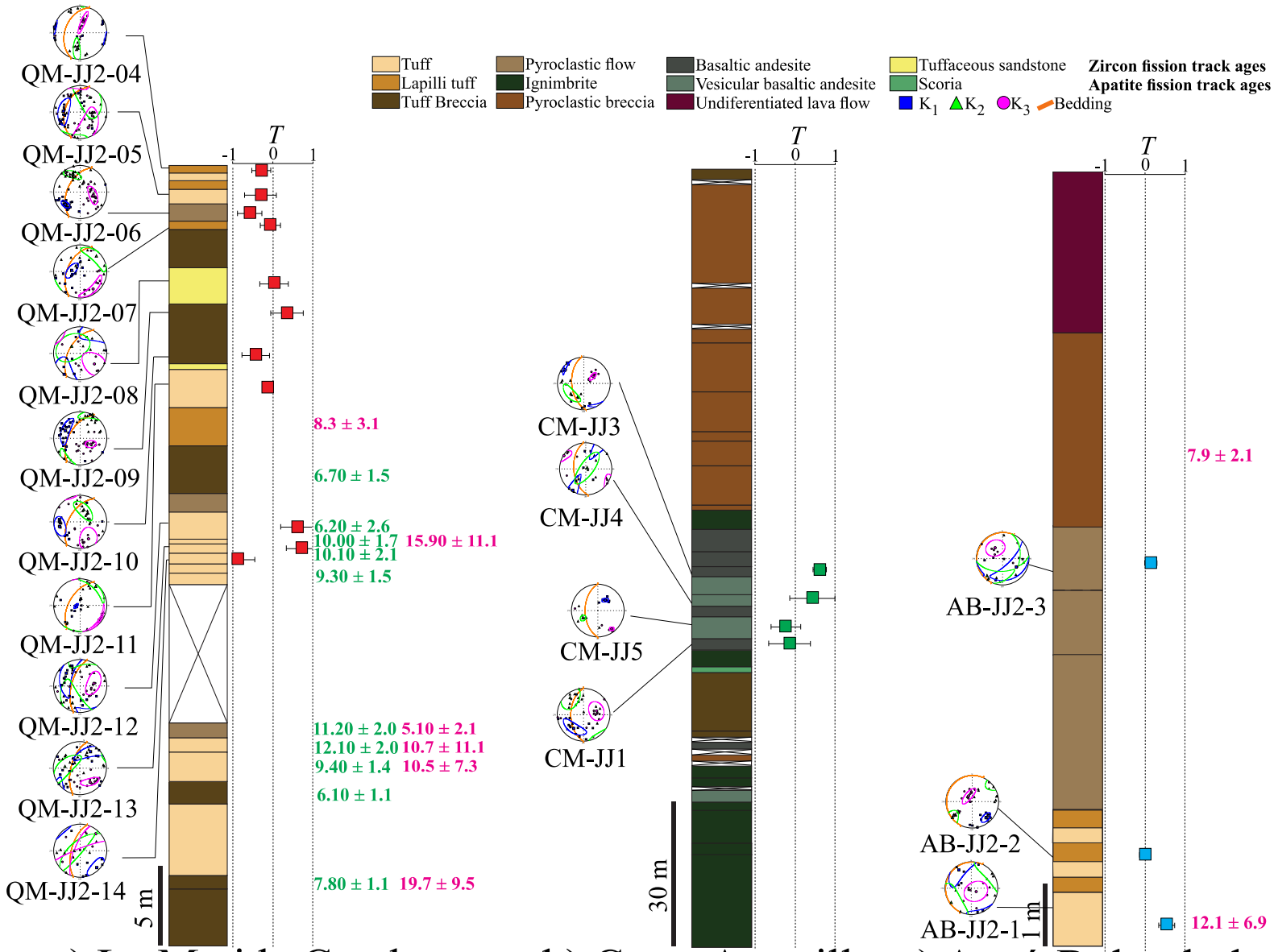
Tuff
Lapilli tuff
Tuff Breccia
Pyroclastic flow
Ignimbrite
Pyroclastic breccia
Basaltic andesite
Vesicular basaltic andesite
Undiferentiated lava flow
Tuffaceous sandstone
Scoria
Zircon fission track ages
Apatite fission track ages
K1 K2 K3 Bedding
T
-1 0 1
QM-JJ2-04
QM-JJ2-05
QM-JJ2-06
QM-JJ2-07
QM-JJ2-08
QM-JJ2-09
QM-JJ2-10
QM-JJ2-11
QM-JJ2-12
QM-JJ2-13
QM-JJ2-14
8.3 ± 3.1
6.70 ± 1.5
6.20 ± 2.6
10.00 ± 1.7
15.90 ± 11.1
10.10 ± 2.1
9.30 ± 1.5
11.20 ± 2.0
5.10 ± 2.1
12.10 ± 2.0
10.7 ± 11.1
9.40 ± 1.4
10.5 ± 7.3
6.10 ± 1.1
7.80 ± 1.1
19.7 ± 9.5
5 m
CM-JJ3
CM-JJ4
CM-JJ5
CM-JJ1
30 m
7.9 ± 2.1
AB-JJ2-3
AB-JJ2-2
AB-JJ2-1
1 m
12.1 ± 6.9
a) La Metida Creek
b) Cerro Amarillo
c) Anzá-Bolombolo

The remaining sites of the CA succession (CA-JJ3 and CA-JJ-5) are characterized by an inversion of the susceptibility axis regarding the sites CM-JJ1 and CM-JJ4. Sites CA-JJ3 and CA-JJ5 have their K_2 axis with SE trends, as the magnetic lineations of the sites CM-JJ1 and CM-JJ4. The site CA-JJ3, which has a well-defined oblate fabric, is characterized by NW-trending sub-horizontal magnetic lineations and a magnetic foliation plane which is dipping towards the SW and has NW-SE strike. On the other hand, the prolate fabric of the site CA-JJ5 has a NE-trending K_1 with an intermediate inclination and a sub-vertical magnetic foliation plane with NE-SW strike (Fig. 4b).

5. Discussion

Magnetic fabric analysis of volcanic and volcano-clastic rocks highly depends on the mineral which carries the magnetic susceptibility (Tarling and Hrouda, 1993; Cañon-Tapia and Pikerton, 2000). We characterize two groups of data according to our k(H) curves and K_m values (Fig. 3a, b). The sampling sites of the MC section are characterized by nonfield-dependent k(H) curves and K_m values mainly between 500×10^{-6} SI and 1000×10^{-6} SI. These features show that the samples of the MC sequence may have their magnetic susceptibility linked to a mixture of ferromagnetic and paramagnetic minerals. On the other hand, sampling sites of the successions AB and CA are characterized by K_m values $>1000 \times 10^{-6}$ SI, which are typical K_m values of ferromagnetic minerals (Rochette, 1987; Borradaile, 1988; Rochette et al., 1992; Borradaile, 2001). There is a slight positive tendency between the applied magnetic field (H) and the bulk magnetic susceptibility (k) for samples of the AB and CA sequences, this behavior can be attributed to the presence of minerals as pyrrhotite, hematite or titanomagnetite (Pokorny et al., 2004). The contribution of these minerals to the magnetic susceptibility do not generate any disturbance in the trends of the AMS axes, however, these minerals can cause inaccurate determination on the degree of anisotropy (Pokorny et al., 2004). We have identified low P_j values for all samples, regardless the k values, therefore, we consider that the possible presence of minerals as pyrrhotite, hematite or titanomagnetite plays no a fundamental role in the interpretation of our AMS data (Fig. 3).

AMS measurements of volcanic and volcano-clastic usually exhibit scattered directions of the mean AMS axes. Therefore, to determine flow directions of these kinds of rocks, a large number of samples is needed and/or it is necessary to studying gathered AMS data from successive flows whose formation and emplacement have similar conditions (Cañon-Tapia et al., 1995; Le Pennec et al., 1998; Cañon-Tapia and Pikerton, 2000; Henry et al., 2003). Due to the analogous lithological and geochronological features of the studied stratigraphic successions, in addition to the similar AMS data between sites of the same section, we have averaged the magnetic directional data of each sequence to obtain reliable results (Fig. 5).

Volcanic vents of the volcanic and volcano-clastic rocks of the Combia Formation have remained unknown. However, volcanic plugs of this unit have to be located within the Amagá Basin, due to the fact that in the adjacent cordilleras there are no records of Mio-Pliocene volcanic events.

The AB succession characterizes sub-horizontal magnetic SE-trending magnetic lineations and a sub-vertical NW-trending K_3. These directions do not present corrections when tilt-corrections are applied, due to the fact that the sequence is only dipping 3°. Usually, the magnetic lineation is coincident with flow directions of volcano-clastic rocks (MacDonald and Palmer, 1990; Palmer et al., 1991; Le Pennec et al., 1998). However, interactions between magnetic grains during the flow, as rolling and saltating, can lead to orthogonal magnetic lineations regarding the flow direction (Porreca et al., 2003; Giordano et al., 2008). For that reason, and considering the ferromagnetic components of the AB section, we have used K_{min} plunge direction to characterize the sense of the flow of this sequence, following the idea of Giordano et al. (2008). Thereby, we have identified flow directions from SE to NW at the AB section, characterizing source areas located in the central area of the Amagá Basin (Fig. 5).

The MC succession presents WSW-trending mean magnetic lineations with an intermediate plunge, whilst K_{min} is oriented towards the SE and has an intermediate plunge. Tilt corrections over these data characterize sub-horizontal magnetic lineations with ENE-WSW trends and sub-horizontal magnetic foliation planes with random strikes. For this sequence, we have used the classical model for magnetic fabrics of volcano-clastic rocks

which displays that magnetic lineation is parallel to the flow direction (Elwood, 1983; MacDonald and Palmer, 1990; Palmer et al., 1991; Le Pennec et al., 1998). We used this statement due to the magnetic mineralogy of the samples of the MC section. K_m values and k(H) curves describe paramagnetic contributions to magnetic fabrics, effects of magnetic interactions as rolling and saltating are not expected in a grain arrangement with paramagnetic minerals, therefore magnetic lineation can be used as an indicator of flow directions for rocks of the MC section. Considering the location of the MC section in the western boundary of the Amagá Basin, flow directions from the ENE towards the WSE are geologically possible (Fig. 5).

Considering the inferred flow directions of the AB and the MC sections, and the lithological and geochronological similitudes between both stratigraphical sequences (Fig. 4a, c), it is possible to determine source areas for these volcano-clastic deposits in the central area of the Amagá Basin. Hypabyssal intrusive rocks of the Combia Event have been thought to be old volcanic necks, due to their geomorphological features which are similar to volcanic cones and previous paleo-current studies (Álvarez, 1983; Ramírez et al., 2006). Based on these statements and the flow directions found for the AB and the MC sections, we deduced that volcanic plugs of the pyroclastic rocks of the central Amagá Basin can be placed in the area of the Venecia town, where a series of cylindrical elevations present morphologies of old volcanoes. The area of Titiribí also has several intrusive rocks of the Combia Event (Fig. 2). Although the intrusive bodies of the Titiribí town do not present well-defined morphologies of volcanoes, it is not discarded that some volcanic plugs would have been located in this area. Following this idea, remnants of volcanic necks in the Titiribí area would have been easily eroded.

The CA section presents a geological history which differs from the origins of the AB and MC successions. The CA sequence, which was sampled at several layers of basaltic andesites, is expected to be close the volcanic vent, due to the fact that lava flows do not travel long distances as pyroclastic deposits. In lava flows, K_1 and K_2 can be parallel to the flow direction (Cañon-Tapia and Pikerton, 2000). We inferred flow directions of these basaltic andesites using oriented vesicles towards the SW. This direction is coincident with

magnetic lineations of the CA sequence, although, in a couple of sampling sites, K_2 axis defines the SW flow direction (Fig. 4b, Fig. 5). These inversions between the AMS axes are common in "natural" lava flows, which are characterized by anisotropy degrees lower than 5%, as the P_j values of the CA section (Cañon-Tapia and Pikerton, 2000).

The location of the CA section in the eastern margin of the Amagá Basin, and the AMS directions, characterize a volcanic plug which would have been closely located to this sequence of lavas. This observation is also corroborated by the magnetic foliation, which characterize planes with similar attitudes to the bedding, showing that lava flows may have flow towards the E-SE (Fig. 5). Despite these analyses related to the CA section, it is necessary to analyze more sites to infer accurate locations for the volcanic plugs which generated the lava flows of the Combia Event.

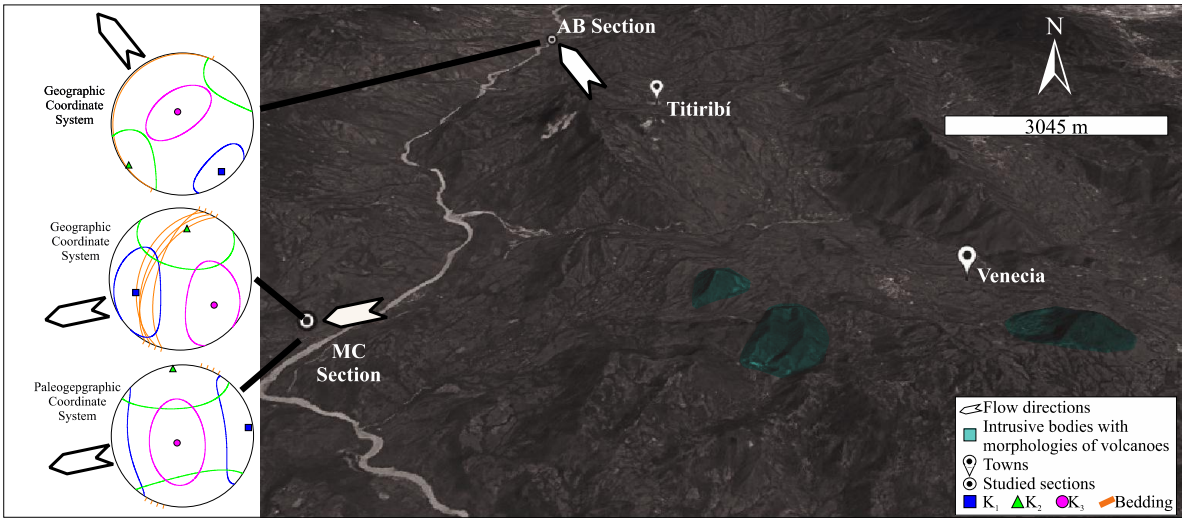

Fig. 5. Oblique aerial view of the study area presenting AMS plots and flow directions of the AB and MC sections. Furthermore, hypabyssal intrusive rocks with geomorphological features of volcanoes are shown. The CA section is not exhibited in this figure due to the fact that we do not clearly identified volcanic plugs for this succession (See text).

Our AMS data characterize flow direction from three successions, however, rocks of the Combia Formation may be records of the deformational events which affected the Amagá Basin during the collisional stages of the PCB and the subsequent reactivation periods of the Cauca-Romeral Fault System. However, we did not find deformational indicators on our magnetic fabrics which can be related to the Late-Cenozoic structural behavior of the

Amagá Basin. Magnetic foliation planes in all three sequences are quite similar to the bedding (Fig. 4), showing that rocks of the Combia Event could be emplaced over a flat topography in the Anzá –Bolombolo sequence and in a steep topography for the remaining sections. However, these facts do not exclude the possibility that the Combia Formation can be a deformed unit. The Amagá Basin is subjected to a strike-slip structural regime which generated rotations in vertical and horizontal axis in the hypabyssal rocks of the Combia Event (Piedrahita et al., 2017b), therefore, further studies are needed to determine effects of deformation on the Combia Formation.

6. Conclusions

The AB and MC sections, which correspond to pyroclastic deposits of the Combia Formation located in the western area of the central Amagá Basin, have their source areas within the basin, in a locality near the hypabyssal rocks of Titiribí or Venecia. However, according to geomorphological features and previous paleo-current studies (e.g. Álvarez, 1983; Ramírez et al., 2006), intrusive rocks of the Venecia area are more likely to be considered as the main volcanic plugs of the central Amagá Basin.

The CA section, which was sampled at lava flows, describes flow directions towards the SW, characterizing volcanic plugs closely placed to this section. However, more studies and sampling locations are needed to accurately determine the volcanic vents which generated lava flows of the CA succession.

Magnetic fabric data of the Combia Formation describe flow directions. Hence, we were not able to detect deformation in these rocks. However, further studies are needed to determine how the Late-Cenozoic deformational events recorded in other rocks of the Amagá Basin, affected the volcanic and volcano-clastic rocks of the Combia Formation.

7. Acknowledgements

The authors thank to Universidad EAFIT (Medellín, Colombia) to make possible the fulfillment of the objectives of this project.

8. References

Acosta, C.A., 1978. El graben interandino Colombo-Ecuatoriano (Fosa Tectónica del Cauca Patía y el corredor Andino-Ecuatoriano). Boletín de Geología Universidad Industrial de Santander 12, 63–75.

Acosta, J., Velandia, F., Osorio, J., Lonergan, L., and Mora, H., 2007. Strike-slip deformation within the Colombian Andes. Geological Society, London, Special Publications 272(1), 303-319.

Álvarez, A., 1983. Geología de la Cordillera Central y el Occidente colombiano y petroquímica de los intrusivos granitoides Mesocenozóicos. Boletín Geológico 26, 175.

Alfonso, C.A., Sacks, P.E., Secor, D.T., Rine, J., Perez, V., 1994. A tertiary fold and thrust belt in the Valle del Cauca Basin, Colombian Andes. Journal of South American Earth Sciences 7, 387–402.

Barrero, D., Pardo, A., Vargas, C.A., Martinez, J.F., 2007. Colombian Sedimentary Basins: Nomenclature, Boundaries and Petroleum Geology, A New Proposal. ANH and B&M Exploration Ltda, Bogotá, Colombia.

Borradaile, G.J, Henry, B., 1997. Tectonic applications of magnetic susceptibility and its anisotropy. Earth Science Reviews 42, 49–93, DOI 10.1016/S0012-8252(96)00044-X

Borradaile, G.J., 1988. Magnetic susceptibility, petrofabrics and strain. Tectonophysics 156, 1–20.

Borradaile, G.J., 2001. Magnetic fabrics and petrofabrics: their orientation distributions and anisotropies. Journal of Structural Geology 23, 1581–1596.

Borrero C. and Toro-Toro L.M., 2016. Vulcanismo de afnidad adaquítica en el miembro inferior de la Formación Combia (Mioceno tardío) al sur de la subcuenca de Amaga, noroccidente de Colombia. Boletín de Geología 38, 87-100.

Buchs, D.M., Arculus, R.J., Baumgartner, P.O., Ulianov, A., 2011. Oceanic intraplate volcanoes exposed: example from seamounts accreted in Panama. Geology 39 (4), 335–338, http://dx.doi.org/10.1130/G31703.1.

Calle, B. and González, H. 1980. Geología y geoquímica de la plancha 166, Jericó Escala 1: 100000, Memoria explicativa. Ingeominas, Bogotá, Colombia.

Calle, B., González, H., de La Peña, D., Escorce, E., Durango, M and others. 1980. Geología de la Plancha 166 Jericó, Escala 1:100000. Ingeominas, Bogotá, Colombia.

Cañón-Tapia, E., Walker, G. P., Herrero-Bervera, E., 1995. Magnetic fabric and flow direction in basaltic pahoehoe lava of Xitle volcano, Mexico. Journal of Volcanology and Geothermal Research 65(3-4), 249-263.

Cañón-Tapia, E., Pinkerton, H., 2000. The anisotropy of magnetic susceptibility of lava flows: an experimental approach. Journal of Volcanology and Geothermal Research 98(1-4), 219-233.

Case, J.E., Duran, L.G., López, A., Moore, W.R., 1971. Tectonic investigations in Western Colombia and Eastern Panama. Geological Society of America Bulletin 82, 2685–2712.

Cediel, F., Shaw, R.P., Cáceres, C., 2003. Tectonic assembly of the Northern Andean Block. In: Bartolini, C., Buffler, R., Blickwede, J. (Eds.), The Circum-Gulf of México and Caribbean: Hydrocarbon Habitats, Basin Formation and Plate Tectonics. American Association of Petroleum Geologists vol. 79, pp. 815–848.

Chadima, M., Jelinek V., 2009. Anisoft 4.2. Anisotropy data browser for Windows. Agico, Inc.

Chicangana, G., 2005. The Romeral fault system: a shear and deformed extinct subduction zone between oceanic and continental lithospheres in Northwestern South America. Earth Science Research 9 (1), 51–66.

Cortés, M., Angelier, J., 2005. Current states of stress in the northern Andes as indicated by focal mechanisms of earthquakes. Tectonophysics 403 (1–4), 29–58. http://dx.doi.org/10.1016/j.tecto.2005.03.020.

Diaz, A., Cuellar, D. 2017, Estratigrafía y geología estructural de la Formación Combia a lo largo de la sección Bolombolo – Concordia. Tesis de pregrado, Universidad Eafit, Medellín, Colombia.

de Boer, J.Z., Defant, M.J., Stewart, R.H., Bellon, H., 1991. Evidence for active subduction below western Panama. Geology 19 (6), 649–652. http://dx.doi.org/10.1130/0091–7613(1991)019b0649:EFASBWN2.3.CO;2.

Duque-Caro, H., 1990. The Choco block in the northwestern corner of South America: structural, tectonostratigraphic, and paleogeographic implications. Journal of South American Earth Sciences 3, 71–84.

Ego, F., Sébrier, M., 1995. Is the Cauca-Patía and Romeral Fault System left or right-lateral? Geophysical Research Letters 22 (1), 33–36.

Elwood, B.B., 1982. Estimates of flow direction for calc-alcaline welded tuffs and paleomagnetic data reliability from anisotropy of magnetic susceptibility measurements: central San Juan mountains, southwest Colorado. Earth and Planetary Science Letters 59, 303– 314

Farris, D.W., Jaramillo, C., Bayona, G., Restrepo-Moreno, A., Montes, C., Cardona, A., Mora, A., Speakman, R.J., Glascock, M.D., Valencia, V., 2011. Fracturing of the Panamanian Isthmus during initial collision with South America. Geology 39, 1007–1010.

Farris, D.W., Cardona, A., Montes, C., Foster, D., Jaramillo, C., 2017. Magmatic evolution of Panama Canal volcanic rocks: a record of arc processes and tectonic change. PloS One 12 (5), e0176010. http://dx.doi.org/10.1371/journal.pone.0176010.

Giordano, G., Porreca, M., Musacchio, P., Mattei, M., 2008. The Holocene Secche di Lazzaro phreatomagmatic succession (Stromboli, Italy): evidence of pyroclastic density current origin deduced by facies analysis and AMS flow directions. Bulletin of Volcanology 70 (10), 1221-1236.

Gansser, A., 1973. Facts and theories on the Andes. Journal of the Geological Society 129, 93–131.

Grosse, E., 1926, Mapa geológico de la parte occidental de la Cordillera Central entre el río Arma y Sacaojal, 1:50000, el terciario Carbonífero de Antioquia, Berlin, Germany.

Henry, B., Plenier, G., Camps, P., 2003. Post-emplacement tilting of lava flows inferred from magnetic fabric study: the example of oligocene lavas in the Jeanne d'Arc Peninsula (Kerguelen islands). Journal of Volcanology and Geothermal Research 127(1-2), 153-164.

Incoronato, A., Addison, F. T., Tarling, D. H., Nardi, G., Pescatore,T., 1983. Magnetic fabric investigations of pyroclastic deposits from Phlegrean Fields, southern Italy. Nature 306, 461–463.

Jaramillo, C., 2016, Evolution of the Isthmus of Panama: biological, paleoceanographic, and paleoclimatological implications. In Hoorn, C., Antonelli, A. (Eds). Mountains, Climate and Biodiversity. Oxford, John Wiley & Sons. 2016EGUGA..18.5020J.

Jelinek, V., 1977. The Statistical Theory of Measuring Anisotropy of Magnetic Susceptibility of Rocks and Its Application. Geofyzika, Brno.

Jelinek, V., 1981. Characterization of the magnetic fabric of rocks. Tectonophysics 79, 63. Ježek, J., Hrouda, F., 2002. Software for modeling the magnetic anisotropy of strained

Kammer, A., 1993. Las fallas de Romeral y su relación con la tectónica de la Cordillera Central. Geología Colombiana 18, 27–46.

Lara, M.E., Silva, J.C., Salazar, A.M., 2015. Early Miocene Accretion of Panamá to Northern South America. Sedimentologic and Geochronologic Evidence from an Intramontane Siliciclastic Succession in the Northwestern Andes. Goldschmidt Conference Abstracts. p. 1675.

Leal-Mejía, H., 2011. Phanerozoic gold metallogeny in the Colombian Andes: a tectono- magmatic approach. PhD Thesis. Universitat de Barcelona, Barcelona, Spain.

Le Pennec, J.-L., Y. Chenn, H. Diot, J.-L. Froger, and A. Gourgaud, Interpretation of anisotropy of magnetic susceptibility fabric of ignimbrites in terms of kinematic and sedimentological mechanisms, An Anatolian case-study., 1998. Earth and Planetary Science Letters 157, 105–127.

MacDonald, W. D., and H. C. Palmer, Flow directions in ash-flow tuffs: A comparison of geological and magnetic susceptibility measurements, Tshirege member (upper Bandelier Tuff) Valles caldera, New Mexico, USA., 1990. Bulletin of Volcanology 53, 45–59.

Mann, P., Corrigan, J., 1990. Model for late Neogene deformation in Panama. Geology (Boulder) 18, 558–562.

Mann, P., Kolarsky, R.A., 1995. East Panama deformed belt: structure, age, and neotectonic significance. In: Mann, P. (Ed.), Geologic and Tectonic Development of the Caribbean Plate Boundary in Southern Central America. Journal of Geophysical Research, Boulder, Colorado, pp. 111–130.

Marín-Cerón, M.I., Bernet, M., Mesa-García, J., 2018. Late Cenozoic to Modern-Day Volcanism in the Northern Andes: A geochronological, petrographical, and geochemical Review. In Cediel, F., Shaw, R.P. (Eds.), Geology and Tectonics of Northwestern South America. Springer.

Mesa-García, J., 2015. Combia Formation: A Miocene Immature Volcanic Arc? Master The- sis. Eafit University, Medellín, Colombia.

Mejía, M., James, M., Arias, L.A., 1988. Evaluación de amenazas geológicas en el área Manizales - Valparaíso. Ingeominas, Medellín, Colombia.

Montes, C., Cardona, A., Jaramillo, C., Pardo, A., Silva, J.C., Valencia, V., Ayala, C., Pérez- Angel, L.C., Rodriguez-Parra, L.A., Ramirez, V., Niño, H., 2015. Middle Miocene closure of the Central American Seaway. Science 348, 226–229.

Nagata, T., 1961. Rock Magnetism. Second Ed Maruzen, Tokyo, Japan.

O'Dea, A., Lessios, H.A., Coates, A.G., Eytan, R.I., Restrepo-Moreno, S.A., Cione, A.L., Collins, L.S., de Queiroz, A., Farris, D.W., Norris, R.D., Stallard, R.F., Woodburne, M.O., Aguilera, O., Aubry, M., Berggren, W.A., Budd, A.F., Cozzuol, M.A., Coppard, S.E., Duque-Caro, H., Finnegan, S., Gasparini, G.M., Grossman, E.L., Johnson, K.G., Keigwin, L.D., Knowlton, N., Leigh, E.G., Leonard-Pingel, J.S., Marko, P.B., Pyenson, N.D., Rachello-Dolmen, P.G., Soibelzon, E., Soibelzon, L., Todd, J.A., Vermeij, G.J., Jackson, J.B.C., 2016. Formation of the Isthmus of Panama. Science Advances 2. http://dx.doi.org/10.1126/ sciadv.1600883.

Ort, M.H., Orsi, G., Pappalardo, L., Fisher, R.V., 2003. Anisotropy of magnetic susceptibility studies of depositional processes in the Campanian Ignimbrite, Italy. Bulletin of Volcanology 65, 55–72.

Palmer, H. C., MacDonald, W. D., Hayatsu, A. 1991. Magnetic, structural and geochronologic evidence bearing on volcanic sources and Oligocene deformation of ash flow tuffs, northeast Nevada. Journal of Geophysical Research: Solid Earth 96(B2), 2185-2202.

Pennington, W.D., 1981. Subduction of the eastern Panama Basin and seismotectonics of northwestern South America. Journal of Geophysical Research B 86, 10753–10770.

Piedrahita, V. A., Bernet, M., Chadima, M., Sierra, G. M., Marín-Cerón, M. I., & Toro, G. E. (2017a). Detrital zircon fission-track thermochronology and magnetic fabric of the Amagá Formation (Colombia): Intracontinental deformation and exhumation events in the northwestern Andes. Sedimentary Geology 356, 26-42.

Piedrahita, V. A., Molina-Garza, R. S., Sierra, G. M., & Duque-Trujillo, J. F. (2017b). Paleomagnetism and magnetic fabrics of Mio-Pliocene hypabyssal rocks of the Combia event, Colombia: tectonic implications. Studia Geophysica et Geodaetica 61(4), 772-800.

Pioli, L., Lanza, R., Ort, M., & Rosi, M. (2008). Magnetic fabric, welding texture and strain fabric in the Nuraxi Tuff, Sardinia, Italy. Bulletin of Volcanology 70(9), 1123-1137.

Porreca M, Mattei M, Giordano G, De Rita D, Funiciello R., 2003. Magnetic fabric and implications for pyroclastic flow and lahar emplacement, Albano maar, Italy. Journal of Geophysical Research 108, DOI 10.1029/2002JB002102

Pokorný, J., Suza, P., Hrouda, F., 2004. Anisotropy of magnetic susceptibility of rocks measured in variable weak magnetic fields using the KLY-4S Kappabridge. In: Martín-Hernández, F., Lüneburg, C.M., Aubourg, C., Jackson, M. (Eds.), Magnetic Fabric: Methods and Applications. Geol. Soc. London, Special Publications, vol. 238, pp. 69–76.

Ramírez, D., López, A., Sierra, G.M., y Toro, G.E. 2006. Edad y proveniencia de las rocas volcánico sedimentarias de la Formación Combia en el suroccidente antioqueño, Colombia. Boletín de Ciencias de la Tierra 19, 9-26.

Restrepo-Moreno, S.A., Foster, D.A., Stockli, D.F., Parra-Sanchez, L.N., 2009. Long-term erosion and exhumation of the "Altiplano Antioqueno," Northern Andes (Colombia) from apatite (U-Th)/He thermochronology. Earth and Planetary Science Letters 278, 1–12, http://dx.doi.org/10.1016/j.epsl.2008.09.037.

Rochette, P., 1987. Magnetic susceptibility of the rock matrix related to magnetic fabric studies. Journal of Structural Geology 9, 1015–1020.

Rochette, P., Jackson, J., Aubourg, C., 1992. Rock magnetism and the interpretation of ansisotropy of magnetic susceptibility. Reviews of Geophysics 30 (3), 209–226.

Sierra, G.M., Marín-Cerón, M.I., 2011. Amagá, Cauca and Patía Basins. In: Cediel, F. (Ed.), Petroleum Geology of Colombia, 2, Fondo Editorial Universidad Eafit, Medellín, Colombia.

Silva, J.C., Sierra, G.M., Correa, L.G., 2008. Tectonic and climate driven fluctuations in the stratigraphic base level of a Cenozoic continental coal basin, northwestern Andes. Journal of South American Earth Sciencies 26, 369–382.

Taboada, A., Rivera, L.A., Fuenzalida, A., Cisternas, A., Philip, H., Bijwaard, H., Olaya, J., Rivera, C., 2000. Geodynamics of the Northern Andes: subductions and intracontinental deformation (Colombia). Tectonics 19, 787–813.

Tarling, D.H., Hrouda, F., 1993. The Magnetic Anisotropy of Rocks. Chapman & Hall, Great Britain.

Van der Hammen, T., 1958. Estratigrafía del Terciario y Maeschtrichiano y Tectonogenesis de los Andes Colombianos. Boletín Geológico Ingeominas 6 (1−13), 67–128.

Villagómez, D., Spikings, R., 2013. Thermochronology and tectonics of the Central and Western Cordilleras of Colombia: Early Cretaceous–Tertiary evolution of the Northern Andes. Lithos 168, 228–249.

Vinasco, C., Cordani, U., 2012. Episodios de reactivación del sistema de fallas del Romeral en la parte Nor-Occidental de los Andes Centrales de Colombia a través de resultados ^{39}Ar-^{40}Ar y K-Ar. Boletín de Ciencias de la Tierra 32, 111–124.

Wegner, W., Wörner, G., Harmon, M.E., Jicha, B.R., 2011. Magmatic history and evolution of the central American land bridge in Panama since the Cretaceous times. Geological Society of America Bulletin 123 (3–4):703–724. http://dx.doi.org/10.1130/B30109.1.

Worm, H.-U., Clark, D., Dekkers, M.J., 1993. Magnetic susceptibility of pyrrhotite: grain size, field and frequency dependence. Geophysical Journal International 114, 127–137.